11-2004

From atomic scale reactant ordering to mesoscale reaction front propagation: CO oxidation on Pd(100)

Da-Jiang Liu
Ames Laboratory, dajiang@fi.ameslab.gov

James W. Evans
Iowa State University, evans@ameslab.gov

From atomic scale reactant ordering to mesoscale reaction front propagation: CO oxidation on Pd(100)

Abstract
We utilize a heterogeneous coupled lattice-gas (HCLG) approach to connect the length scales from a realistic atomistic description of surface reactions to the associated mesoscale spatiotemporal behavior. This method is applied to describe reaction front structure in a model for CO oxidation on Pd(100) which incorporates complex ordering of CO and O adlayers, and a precise treatment of the chemical diffusion for interacting CO adlayers in an environment of coadsorbed O.

Keywords
carbon, palladium, chemical environment, chemical structure, diffusion, nuclear reactor, oxidation

Comments
This article is from *Physical Review B* 70 (2004): 193408, doi: 10.1103/PhysRevB.70.193408. Posted with permission.

From atomic scale reactant ordering to mesoscale reaction front propagation: CO oxidation on Pd(100)

Da-Jiang Liu[1] and J. W. Evans[1,2]
[1]*Ames Laboratory—USDOE, Iowa State University, Ames, Iowa 50011, USA*
[2]*Department of Mathematics, Iowa State University, Ames, Iowa 50011, USA*
(Received 18 June 2004; published 16 November 2004)

We utilize a heterogeneous coupled lattice-gas (HCLG) approach to connect the length scales from a realistic atomistic description of surface reactions to the associated mesoscale spatiotemporal behavior. This method is applied to describe reaction front structure in a model for CO oxidation on Pd(100) which incorporates complex ordering of CO and O adlayers, and a precise treatment of the chemical diffusion for interacting CO adlayers in an environment of coadsorbed O.

DOI: 10.1103/PhysRevB.70.193408 PACS number(s): 68.43.Jk, 68.43.Mn, 82.40.Np, 82.65.+r

A common feature of diverse reaction-diffusion systems is that chemical reaction processes occurring on a local atomic scale couple with diffusive transport processes produce spatiotemporal pattern formation, observable on a much larger scale.[1,2] The classic example from three-dimensional (3D) solution-phase reactions is the unstirred Belousov-Zhabotinskii reaction exhibiting a macroscale spiral wave formation. More recently, developments in ultrahigh-vacuum (UHV) surface-sensitive microscopy techniques have allowed *in situ* analyses of mesoscale reaction front propagation in 2D catalytic surface reactions such as CO oxidation.[3] In fact, CO oxidation provides a well-controlled environment to elucidate an extraordinary variety of spatiotemporal behaviors in relatively simple reaction systems.

Traditionally, these systems are analyzed by reaction-diffusion equations which combine mean-field rate equations (describing well-stirred reactants) for chemical kinetics with a simplified treatment of transport.[1–3] The latter assumes Fickian diffusion with constant diffusion coefficients, and ignores coupling between diffusive flux of one reactant and gradients of other reactants. This approach is reasonable for bulk reactions, and has also been quite successful in elucidating surface reaction phenomena. However, for the latter chemisorption systems, it is clear that reactant ordering or islanding due to adspecies interactions, and limited mobility of some adspecies, invalidate the mean-field assumption.[4] Also diffusion coefficients have strong coverage or concentration dependence, and coupling between transport of different adspecies is enhanced in 2D.[5] Recent mesoscale modeling of such pattern formation has incorporated coverage-dependent diffusivity, but still treats reaction and transport at a mean-field level.[6] Thus, there is motivation to develop an approach to connect a realistic atomistic description of reaction and transport properties to a mesoscale description of reaction front propagation (where the characteristic length scale is on the order of microns).

A number of generic strategies have been proposed to meet this challenge of connecting the length scales. For systems where reactants reside at a periodic array of crystalline sites, a heterogeneous-coupled-lattice-gas (HCLG) technique has been proposed.[5,7] Here, the local reaction kinetics and transport parameters for different heterogeneous macroscopic points distributed across the reaction front are analyzed in parallel via kinetic Monte Carlo (KMC) simulation of the appropriate lattice-gas models. These parallel simulations are then appropriately coupled to reflect mesoscale mass transport between the macroscopic points. An analogous technique, the so-called gap tooth method (GTM), has been discussed mainly in the context of hydrodynamics.[8] The "teeth" are the microdomains described simultaneously by particle simulation, and these are coupled by suitable hydrodynamic fluxes. HCLG and GTM constitute examples of more general heterogeneous multiscale methods (HMM) (Ref. 9) which couple microscopic with macroscopic computational domains, and can be applied to a host of different physical problems, e.g., gas-phase kinetic theory, interfacial dynamics, homogenization problems.

However, a major challenge is the application of these multiscale methods to treat realistic models for specific complex systems. For reaction-diffusion systems, this requires not just incorporating a realistic atomistic treatment of reaction processes, but also analyzing the complex many-body nature of diffusive transport. The latter feature is due to interactions among the diffusing species themselves, and with other coreactants. This feature has not been incorporated into previous multiscale modeling.

In this Brief Report, we use the HCLG method to provide such an analysis of mesoscale reaction front propagation for CO oxidation on a Pd(100) surface under UHV (Ref. 10) (rather than high pressure[11]) conditions. Analysis is based on a realistic atomistic model which we developed to describe not just the complex ordering observed separately for CO and O adlayers on Pd(100), but also the structure of mixed adlayers which will impact reaction kinetics. This model predicts bistability between a reactive state with low CO coverage and an inactive near-poisoned state with high CO coverage. We also develop a KMC algorithm which can simultaneously extract "exact functional forms" for both reaction kinetics and CO diffusivity from the atomistic model. Furthermore, we present a refined algorithm for stationary fronts, and discuss general speed-up procedures for the HCLG simulations. We then apply the model and algorithm to describe the mesoscale front or chemical wave between the bistable states, focusing on stationary front structure.

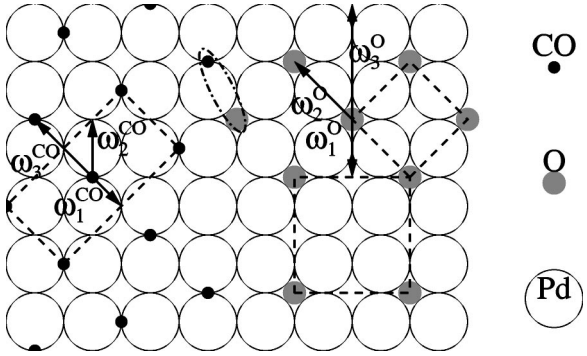

FIG. 1. Schematic of local $c(2\sqrt{2}\times\sqrt{2})R45°$ ordering of CO/Pd(100), together with CO-CO interactions. Also shown is local $c(2\times2)$ (upper right) and $p(2\times2)$ (lower right) ordering of O/Pd(100) together with O-O interactions. A CO-O pair which can react with rate k is also shown.

We now describe in some detail the key components of our realistic atomistic LG model for CO oxidation on Pd(100) with the surface lattice constant denoted below by "a." Adspecies interactions are fine-tuned so that the model recovers observed equilibrium adlayer ordering, a feature not guaranteed by adopting values from *ab initio* calculations using standard approximations. We also note that specification of kinetics is critical in determining local ordering under *nonequilibrium* reaction conditions. As an aside, we note that realistic LG modeling has long been used to describe equilibrium ordering in chemisorbed layers,[12] and recently in studies of titration of preadsorbed O on Pt(111) by exposure to CO.[13,14]

Adspecies interactions and equilibrium ordering (see Fig. 1). For equilibrated CO/Pd(100) adlayers, CO sits at bridge sites and displays a $c(2\sqrt{2}\times\sqrt{2})R45°$ ordered structure for CO coverage θ_{CO} around 0.5 ML, with a commensurate-incommensurate transition possible at higher θ_{CO}.[15,16] Our model recovers this ordering, as well as experimental behavior related to CO adsorption. This is achieved using binding energy of $\epsilon_0=1.60$ eV for isolated CO, and the following pairwise CO-CO interactions: strong (exclusive) repulsion $\omega_1^{CO}=\infty$ for sites separated by $a/\sqrt{2}$, repulsion $\omega_2^{CO}=0.17$ eV for separation a, weak repulsion $\omega_3^{CO}=0.02$ eV for separation $\sqrt{2}a$. For equilibrated O/Pd(100) adlayers, O sits at hollow sites and displays transition from disorder to $p(2\times2)$ ordering to $c(2\times2)$ ordering with increasing O coverage $\theta_O(\leqslant0.5$ ML).[17] To model this behavior, we impose pairwise O-O interactions including strong (exclusive) repulsions $\omega_1^O=\infty$ for nearest-neighbor (NN) sites separated by a [giving rise to $c(2\times2)$ ordering], and finite repulsions $\omega_2^O=0.13$ eV>0 for second-nearest-neighbor (2NN) sites separated by $\sqrt{2}a$. We include additional attractions $\omega_3^O=-0.03$ eV for third-nearest neighbor (3NN) sites separated by $2a$ to stabilize and expand the existence region of the $p(2\times2)$ phase to match experiments.

CO adsorption, diffusion, and desorption dynamics. Motivated by DFT studies showing steering of adsorbing CO to on-top sites,[18] we first attempt to deposit CO at an on-top site, then at one of neighboring bridges sites if the on-top is unavailable, then at one of the hollow sites if the bridges are unavailable. (Availability means avoiding double occupancy and exclusive repulsive interactions.) Subsequent hopping from on-top or hollow sites to bridge sites is irreversible at rate h_{CO}; hopping between neighboring bridge sites occurs at a rate $h_{CO}\min\{1,e^{-\Delta E/kT}\}$, where ΔE denotes the energy change based on adspecies interactions. Bridge-to-bridge hopping produces mesoscale CO mass transport, since h_{CO} is many orders of magnitude above other rates. We will perform simulations with large h_{CO} to extract relevant behavior of local quantities, and then use the HCLG procedure to directly model reaction fronts on the length scale $\sim(h_{CO})^{1/2}$. Finally, CO can desorb nonreactively from the surface with a rate determined by a desorption barrier $\epsilon_d=\epsilon_0-\omega_{int}$, where $\omega_{int}\geqslant0$ denotes the sum of repulsive adspecies interactions.

O adsorption and diffusion dynamics. Dissociative adsorption of O_2 on Pd(100) occurs via an eight-site rule reflecting the NN repulsions $w_1^O=\infty$: O atoms deposit at 2NN hollow sites, provided these are empty and all six additional NN hollow sites are also free of O.[19] In addition, we avoid double occupancy and exclusive repulsions with CO (see below). A small amount of O mobility (relative to CO) exists and impacts local structure, e.g.; generating local $p(2\times2)$ ordering. Thus, we include O hopping to neighboring hollow sites at a rate $h_O\min\{1,e^{-\Delta E/kT}\}$.

CO+O *interaction and reaction dynamics*. We exclude CO from the four bridge sites adjacent to an O due to strong repulsions. This facilitates entropically driven separation into ordered CO and O domains, a feature which is believed to characterize this reaction system.[10] We let O react with CO on a 2NN bridge site a distance $\sqrt{5}/2a$ away, or with CO on neighboring hollow or on-top sites. Different prescriptions of the reaction rate k are possible. Suppose that the activation barrier reflects adspecies interactions being lowered by repulsions (as is the desorption barrier ϵ_d). Then a low population of reactants in high-energy states interior to coreactant domains is counterbalanced by a higher reaction rate, which tends to make the CO_2 production rate spatially uniform. Instead, if the activation barrier is insensitive to adspecies interactions, then CO_2 production occurs primarily along boundaries between O and CO domains. The latter scenario is expected for CO+O/Pd(100),[10] and is thus chosen here.

Note that the choice of Metropolis-like rates for diffusion of CO and O is certainly an idealization. We have explored other schemes for specifying hopping rates, which can yield different behavior, e.g., for CO diffusivity. However, results presented below are quite representative.

Model results are presented below for CO oxidation on Pd(100) at 390 K where we estimate that $k\approx1$ s^{-1} [assuming a barrier of 1.0 eV (Ref. 20)]. Prefactors for Arrhenius rates are chosen as 10^{13} s^{-1}. For simplicity, we assume that reactant partial pressures (of the order 10^{-3} Torr) are adjusted so that the total adsorption rate for the clean surface satisfies $p_{CO}+p_{O_2}=1$ (in units of s^{-1}). Finally, we note that provided O is mobile on the time scale of deposition and reaction, results are not sensitive to the precise choice of h_O. Figure 2 shows simulation results for steady-state behavior adopting an algorithm where one specifies θ_{CO}, and extracts the corresponding p_{CO}.[21] This approach demonstrates not just the development of bistability with increasing h_{CO}, but also pre-

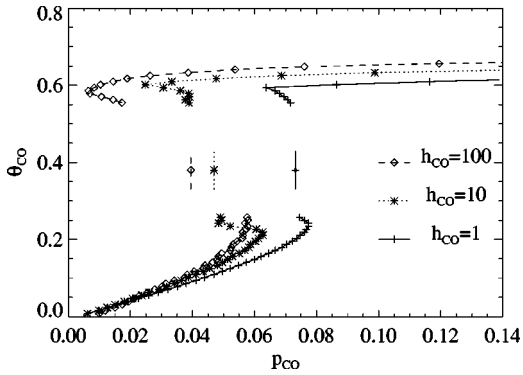

FIG. 2. Steady-state behavior for θ_{CO} vs p_{CO} for $h_{CO}=1$, 10, and 100. Results from constant- θ_{CO} simulations (Ref. 21) in a 128 $\times$128 site system. Results for $\theta_{CO}\approx 0.4$ reflect equistability pressures between the bistable states.

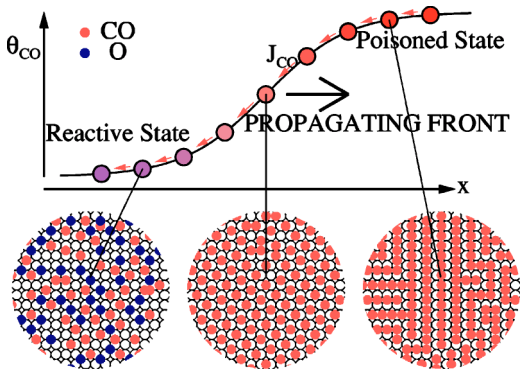

FIG. 3. (Color online) Schematic of the HCLG procedure. Expanded views of macroscopic points across the reaction front show simulated adlayer distributions during CO oxidation on Pd(100). CO=red, O=blue. Propagation shown for p_{CO} below p_{CO}^{eq}.

dicts the equistability pressure p_{CO}^{eq}, where reactive and inactive states are equally stable. We find that $p_{CO}^{eq}\approx 0.04$ for large h_{CO}.

Next, we examine the structure of planar reaction-diffusion fronts separating the reactive and inactive states in the bistable region. We focus on the physically relevant hydrodynamic regime of large h_{CO}, where these fronts are described by an exact reaction-diffusion equation (RDE) of the form

$$\partial\,\theta_{CO}/\partial\,t = R_{CO}(\theta_{CO},\{O\}) - \nabla\cdot\boldsymbol{J}_{CO}, \tag{1}$$

together with rate equations for the oxygen coverage and for various spatial correlation functions related to the oxygen adlayer. The "bistable kinetics" term R_{CO} includes gain contributions from deposition and loss from reaction and desorption. The specific form of such terms reflects the adlayer ordering which is determined by not just the coverage of locally equilibrated CO, but by the actual distribution $\{O\}$ of O. Mesoscale diffusion for O is absent, and for CO is described by the flux

$$\boldsymbol{J}_{CO} = -(kT)^{-1}\sigma_{CO}\theta_{CO}\nabla\,\mu_{CO}(\theta_{CO},\{O\}) = -\sigma_{CO}S^{-1}\nabla\,\theta_{CO}, \tag{2}$$

where μ_{CO} is the chemical potential of locally equilibrated CO and σ_{CO} is the CO mobility (determined from the displacement of the center of mass $\boldsymbol{R}_{c.m.}$ of the CO particles in a finite system with periodic boundary conditions). Also, $S^{-1}=(kT)^{-1}\theta_{CO}d\mu_{CO}/d\theta_{CO}$, is determined by measuring fluctuations in θ_{CO}. Here $d/d\theta_{CO}$ represents a total derivative for states along the reaction front. We emphasize that this analysis incorporates the effects of interactions and coadsorbed O on CO diffusion.

In the HCLG procedure, simulations at macroscopic "points" distributed uniformly across the front simultaneously determine R_{CO},σ_{CO}, and fluctuation quantities. These simulations are periodically coupled to transport CO between adjacent "points" at a rate determined by J_{CO}, using a standard discrete approximation for $\nabla\theta_{CO}$. This approach is analogous to the "method of lines" treatment of mean-field RDE's, except that we replace mean-field rate equations describing the kinetics at each macroscopic "point" with LG simulations (and also use these simulations to precisely determine transport). Simulations could start with a sharp front which quickly relaxes to its selected profile. Figure 3 shows a "schematic" of this procedure, which incorporates actual adlayer distributions at various macroscopic points across the front, as determined from LG simulations.

Rather than general analysis of reaction front behavior, here we focus on structure at the equistability point $p_{CO}^{eq}=0.04$, where the front is stationary, so $\partial\theta_{CO}/\partial t=0$ in Eq. (1). In this case, we have developed a novel LG simulation algorithm to extract the needed quantities *independently* for each macroscopic point across the front. In this algorithm, we set a target CO coverage θ_{CO}^{*}, then perform a standard simulation, but periodically check the actual θ_{CO} value, and add or remove CO to maintain the target θ_{CO}^{*}. During the simulation, we monitor this flux of added/removed particles $F_{CO}(\theta_{CO}^{*})=\nabla\cdot\boldsymbol{J}_{CO}=R_{CO}(\theta_{CO}^{*},\{O\})$, as well as the CO mobility and fluctuations. The dependence on θ_{CO}^{*} of key quantities, as well as of the diffusion coefficient $D_{CO}=\sigma_{CO}S^{-1}$, is shown in Fig. 4. Note that R_{CO} with its three zeroes (or stationary points) has the generic form for a bistable system.[1]

Finally, from the variation of R_{CO} and D_{CO} with θ_{CO} across the front at the equistability point, determined above,

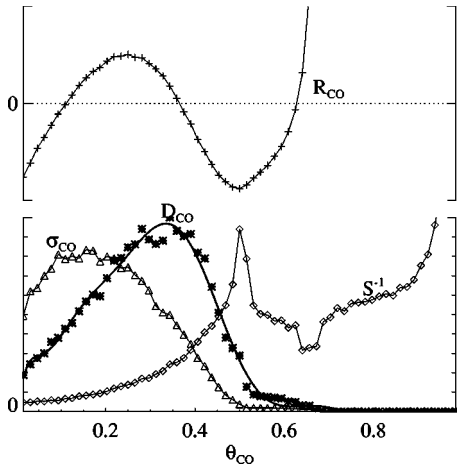

FIG. 4. R_{CO} (top), S^{-1},σ_{CO}, and D_{CO} (bottom) vs θ_{CO} across the reaction front at equistability $p_{CO}=0.04$. In arbitrary units.

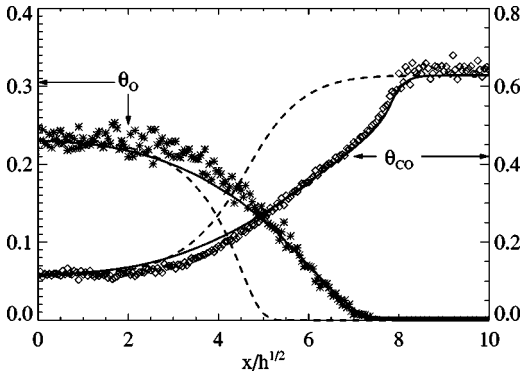

FIG. 5. θ_{CO} and θ_O profiles across the reaction front at equistability. Results from the exact RDE (solid line) vs mean-field RDE (dashed line). Symbols show results from direct simulation.

we can simply integrate the steady-state RDE to obtain the coverage profile across the front. Figure 5 shows the results of this analysis as compared against results for the coverage profile obtained from direct LG simulations with finite but large h_{CO} on a very large lattice. It is clear that results from the exact RDE recover the results from direct (and expensive) LG simulation, demonstrating the validity of the approach for realistic reaction models. Results using the same "exact" reaction kinetics, but with a constant diffusion coefficient, are shown by dashed lines. It is clear that correct diffusivity is required for reproducing the wave front structure using HCLG procedures.

In conclusion, much recent effort has been directed towards modeling of pattern formation in surface reaction systems addressing the challenges of rapid diffusion and complex local self-organization.[6,22,23] In contrast to these works, we present a multiscale analysis based on a realistic model for atomistic ordering and reaction kinetics for a specific reaction system, CO oxidation on Pd(100). Instead of the HCLG procedure, one could also analyze this system by scaling up simulations with lower CO hop rates (see Fig. 5). However, such a brute-force simulation is a "black-box" approach which cannot provide insight into the detailed form of spatial patterns and the underlying features of transport properties. Furthermore, the HCLG procedure is amenable to dramatic "speed up" by exploiting analytic treatments of the CO mobility, and replacing conventional simulation of locally equilibrated CO distributions, fluctuations, and reaction kinetics by "artificial dynamics" (which preserves the correct equilibrium structure). Finally, we note that the HCLG procedure can be readily applied to distribution of the individual parallel LG simulations on clusters or grids of processors.

This work was supported by the Division of Chemical Sciences, USDOE-BES. It was performed at Ames Laboratory, operated for the USDOE by ISU under Contract No. W-7405-Eng-82.

[1] A. S. Mikhailov, *Foundations of Synergetics I: Distributed Active Systems* (Springer-Verlag, Berlin, 1994).
[2] *Chemical Waves and Patterns*, edited by R. Kapral and K. Showalter (Kluwer, Dordrecht, 1995).
[3] R. Imbihl and G. Ertl, Chem. Rev. (Washington, D.C.) **95**, 697 (1995).
[4] T. Engel and G. Ertl, Adv. Catal. **28**, 1 (1979).
[5] J. W. Evans, D.-J. Liu, and M. Tammaro, Chaos **12**, 131 (2002).
[6] M. Hildebrand, A. S. Mikhailov, and G. Ertl, Phys. Rev. Lett. **81**, 2602 (1998).
[7] M. Tammaro, M. Sabella, and J. W. Evans, J. Chem. Phys. **103**, 10277 (1995).
[8] C. W. Gear, J. Li, and I. G. Kevrekidis, Phys. Lett. A **316**, 190 (2003).
[9] W. E and B. Engquist, Commun. Math. Sci. **1**, 87 (2003).
[10] E. M. Stuve, R. J. Madix, and C. R. Brundle, Surf. Sci. **146**, 155 (1984).
[11] B. L. M. Hendriksen, S. C. Bobaru, and J. W. M. Frenken, Surf. Sci. **552**, 229 (2004).
[12] W. H. Weinberg, Annu. Rev. Phys. Chem. **34**, 217 (1983).
[13] S. Völkening and J. Wintterlin, J. Chem. Phys. **114**, 6382 (2001).
[14] J. Wintterlin, S. Völkening, T. V. W. Janssens, T. Zambelli, and G. Ertl, Science **278**, 1931 (1997).
[15] R. J. Behm, K. Christmann, G. Ertl, and M. A. Van Hove, J. Chem. Phys. **73**, 2984 (1980).
[16] R. Schuster, I. K. Robinson, K. Kuhnke, S. Ferrer, J. Alvarez, and K. Kern, Phys. Rev. B **54**, 17 097 (1996).
[17] S.-L. Chang and P. A. Thiel, J. Chem. Phys. **88**, 2071 (1988).
[18] A. Eichler and J. Hafner, Phys. Rev. B **57**, 10 110 (1998).
[19] S.-L. Chang and P. A. Thiel, Phys. Rev. Lett. **59**, 296 (1987).
[20] C. J. Zhang and P. Hu, J. Am. Chem. Soc. **123**, 1166 (2001).
[21] R. M. Ziff and B. J. Brosilow, Phys. Rev. A **46**, 4630 (1992).
[22] O. Kortluke, V. N. Kuzovkov, and W. von Niessen, Phys. Rev. Lett. **83**, 3089 (1999).
[23] R. M. Nieminen and A. P. J. Jansen, Appl. Catal., A **160**, 99 (1997).